Journal of Electroanalytical Chemistry 896 (2021) 115199

Contents lists available at ScienceDirect

Journal of Electroanalytical Chemistry

journal homepage: www.elsevier.com/locate/jelechem

Oxide-oxide galvanic displacement reactions: Effect of the concentration of the ions released by the sacrificial oxide

Nicola Comisso [a], Lidia Armelao [b,c], Sandro Cattarin [a], Stefano Fasolin [a], Luca Mattarozzi [a], Marco Musiani [a,*], Marzio Rancan [d], Lourdes Vázquez-Gómez [a], Enrico Verlato [a]

[a] ICMATE CNR, Corso Stati Uniti 4, 35127 Padova, Italy
[b] Dipartimento di Scienze Chimiche, Università di Padova, Via Marzolo 1, 35121 Padova, Italy
[c] DSCTM CNR, Piazzale Aldo Moro 7, 00185 Roma, Italy
[d] ICMATE CNR, Via Marzolo 1, 35121 Padova, Italy

ARTICLE INFO

Keywords:
Galvanic replacement
Gas bubble templated deposition
Mixed oxides
PbO_2
Porous electrodes

ABSTRACT

Galvanic displacement reactions between a solid oxide and a dissolved metal cation are interesting processes for the preparation of oxide nanoparticles or electrocatalytic layers consisting of secondary mixed oxides. Their mechanism is not yet fully clarified. The composition of the secondary mixed oxides and their growth rate depend on many physical and chemical variables. In the present study, we have focused on the effects of the concentration of the ions released from the sacrificial oxide to the solution, when they are intentionally added to reaction media. We have studied the displacement of sacrificial PbO_2 by either Mn^{2+} or Co^{2+} cations in acetate solution that contained variable concentrations of Pb^{2+}, using electrochemical methods, SEM-EDS and XPS. The evolution of the open circuit potential of the systems was monitored during the reactions. We have found that, for both divalent cations, increasing concentrations of Pb^{2+} ions in the acetate solutions caused the formation of mixed oxides richer in Pb. Effects on growth rate and equilibrium potential were different for Mn^{2+} and Co^{2+}.

1. Introduction

The displacement of a metal by the cations of a nobler one, a common process that may lead to detrimental metal corrosion or be useful in metal recovery [1], has been often exploited as a key step in the preparation of nano-stuctured catalytic materials [2,3]. Comparable reactions involving a sacrificial oxide, which undergoes dissolution, and a metal cation which forms a secondary oxide have attracted attention during the last decade, being used to produce oxide nanoparticles with complex structures [4–15] or electrocatalytic layers for the oxygen evolution reaction [16–19]. In galvanic displacement reactions, the sacrificial metal always undergoes oxidation. Instead, in analogous processes, a sacrificial oxide may be either oxidized [4,9,10] or reduced [5–8,10–19].

Our group has investigated the little-known mechanism of oxide-oxide galvanic displacement reactions, using sacrificial PbO_2 layers, either compact or porous, and various cations (Mn^{2+}, Co^{2+}, Ni^{2+}, Fe^{2+}, Sn^{2+}), reaching the following main conclusions [18]:

(i) The diffusion of Pb species across secondary oxides controls their growth rate which does not correlate in any simple way with the thermodynamic driving force of the reaction.
(ii) Secondary oxides formed on top of PbO_2 contain more or less significant amounts of the sacrificial oxide metal, i.e. they are mixed oxides. The stoichiometry of a galvanic displacement reaction between PbO_2 and a generic metal cation M^{n+}, leading to a mixed M−Pb oxide, is shown in the Supplementary Information.
(iii) Tertiary layers may be grown on secondary oxides. The growth occurs at the interface between the outermost layer and the solution. This suggests that the inwards diffusion of cations to reach the sacrificial oxide surface is not necessary.
(iv) In most cases, secondary oxides are amorphous. Only using Fe^{2+} as cation, the formation of agglomerates of crystalline FeOOH platelets was observed on top of an amorphous layer of similar chemical composition [19].

* Corresponding author.
E-mail address: marco.musiani@cnr.it (M. Musiani).

https://doi.org/10.1016/j.jelechem.2021.115199
Received 15 February 2021; Received in revised form 19 March 2021; Accepted 22 March 2021

Typical experimental conditions used in our previous studies on oxide-oxide galvanic displacement reactions involved the use of the same 50 mL volume of divalent cation solution in a series of 15–20 successive tests during which Pb^{2+} ions were produced upon PbO_2 reduction and released to the solution. Since the mass of PbO_2 used in each experiment was ca. 0.6 mg, assuming its total dissolution, after 20 experiments the concentration of Pb^{2+} ions would rise to ca. 0.001 M. However, experimental evidence showed that PbO_2 was only partially displaced [16–19], to an extent that depended on the nature and concentration of the reducing cation, the solution temperature and the duration of the reaction. Thus, the Pb^{2+} ions concentration was still well below 0.001 M when the solutions were disposed. Such a concentration of Pb^{2+} was assumed to be uninfluential on the displacement reactions and possible memory effects were disregarded. The effect of significantly higher concentrations of Pb^{2+} was not investigated in our previous work and is addressed in the present paper. The new evidence that we have collected improves our understanding of the mechanism of oxide-oxide galvanic displacement reactions and further supports previous conclusions.

2. Material and methods

Porous PbO_2 layers were deposited on Au screen printed electrodes (0.125 cm^2 geometric area, purchased from Dropsens), from methanesulfonic acid baths, using the oxygen bubble templated anodic deposition method [20,21]. In each deposition, a two-step electrolysis was performed, respectively at low (10 mA cm^{-2}) and high (1 to 3 A cm^{-2}) current densities, to obtain first a thin compact PbO_2 layer, which homogeneously coated the Au electrode and ensured adhesion, and then a thicker porous layer. An Autolab PGSTAT 302N was used to perform the electrolyses in a single compartment cell, with a Pt wire counter electrode.

The galvanic displacement reactions were performed by immersing PbO_2-coated screen printed electrodes in acetate buffers (pH 4.8) containing either Mn^{2+} or Co^{2+} cations. The compositions of these solutions were: 0.20 M $Mn(CH_3COO)_2$, 0.20 M CH_3COOH and 0.20 M $Co(NO_3)_2$, 0.02 M CH_3COOH, 0.20 M $NaCH_3COO$, respectively [16,18]. The former was used at 25 °C and the latter at 75 °C to grow secondary layers with comparable thicknesses for reaction durations (t_{ge}) of 60 min. Both solutions contained up to 0.1 M Pb^{2+} ions. The open circuit potential of the samples was monitored during galvanic displacement reactions, using an EG&G PAR 263A apparatus, with respect to an Ag/AgCl reference electrode connected to the main compartment via a salt bridge. In the following sections, potentials are referred to SHE.

The resulting oxide layers were characterized by SEM-EDS and XPS. A Zeiss SIGMA instrument, equipped with a field emission gun, operating under high vacuum conditions at an accelerating voltage variable between 10 and 30 kV, was used to obtain SEM images. Energy Dispersive Spectroscopy analyses were performed with an Oxford X-MAX apparatus. XPS analyses were performed with a Perkin-Elmer F 5600-ci spectrometer using Al Kα radiation (1486.6 eV). Further details may be found in [16–18].

3. Results and discussion

3.1. PbO_2-Mn^{2+} reaction – SEM-EDS and XPS characterization

The main reaction chosen for this study was the displacement of PbO_2 by Mn^{2+}, where the oxide underwent partial reduction and the cations present in solution underwent oxidation to a solid oxide. This reaction may be written:

$$PbO_2 + xMn^{2+} \rightarrow Mn_xPb_{(1-x)}O_2 + xPb^{2+} \quad (1)$$

Further details on the reaction stoichiometry may be found in the Supplementary Information. In our experience, this reaction was the easiest to investigate experimentally because its rate was rather high at room temperature. Furthermore, its stoichiometry was the simplest because the metal/oxygen ratio was maintained during the displacement. To investigate how the concentration of Pb^{2+} ions intentionally added to the Mn^{2+} solutions used in galvanic displacement reactions affected the composition and growth rate of the secondary oxides, we employed porous PbO_2 layers essentially identical to those used in our previous studies aimed at obtaining enhanced charge capacity [22] or, when Co^{2+} [16–18], Ni^{2+} [18] or Fe^{2+} [19] were used instead of Mn^{2+}, at preparing large-surface-area electrocatalytic layers.

The SEM images in Fig. 1 show the effect of $[Pb^{2+}]$ on the morphology of $PbO_2/Mn_xPb_{(1-x)}O_2$ samples obtained with 60-min reactions. At low concentration, the Pb^{2+} ions intentionally added to the Mn^{2+} solutions did not alter the aspect of the samples which were porous due to the shaping action of the oxygen bubbles evolved during high-rate anodic deposition of PbO_2. After galvanic displacement, both in the absence of Pb^{2+} and with $[Pb^{2+}] = 10$ mM, the porous PO_2 was coated by globular secondary oxide deposits, normally less than 1 μm wide, with some additional smaller features irregularly distributed on the outermost parts of the samples, as already observed [16]. These smaller features were not visible when the Pb^{2+} concentration was increased to 30 or 100 mM. In these cases, the aspect of pristine porous PbO_2 deposit [20,21] was less markedly modified by the secondary oxide which formed conformal layers.

Fig. 2 shows cross sectional images of three samples prepared with different Pb^{2+} concentrations and identical 60 min durations of the displacement reactions. In all cases, $Mn_xPb_{(1-x)}O_2$ layers were detected, which coated both the outer and the inner parts of the large pores. Their thickness was rather homogeneous in different parts of each sample, but depended on Pb^{2+} concentration. While the secondary oxide thickness was very similar for $[Pb^{2+}] = 1$ or 10 mM, being always close to 2.2 μm, it markedly decreased to ca. 0.9 μm when $[Pb^{2+}]$ was increased to 100 mM. Thus, the average growth rate decreased from ca. 35 to ca. 15 nm min^{-1}. One may speculate that the disappearance of small, irregular features at high $[Pb^{2+}]$, see Fig. 1, was caused by a slower, more regular growth than in Pb^{2+}-free solutions. In Fig. 2, images obtained with the same magnification are compared. The thin $Mn_xPb_{(1-x)}O_2$ layer formed with $[Pb^{2+}] = 100$ mM is better visible in Fig. S1 of the Supplementary Information.

Analogous SEM analyses were performed on samples prepared with shorter reactions (10 min). The images in Fig. S2 (Supplementary Information), relevant to samples obtained with $[Pb^{2+}] = 1$ mM or 100 mM, show that a thinner secondary oxide layer was obtained at the higher Pb^{2+} concentration, also in this case. In the absence of Pb^{2+} in solution, the average growth rate during the initial 10 min period was close to 70 nm min^{-1}, about twice the value averaged over 60 min, due to progressive decrease of the diffusion rate resulting from secondary oxide thickening.

By averaging the values measured at no less than 5 different positions for each sample, the $[Pb^{2+}]$-thickness plots shown in Fig. 3 were obtained. For both reaction durations, the lowest thicknesses were obtained at the highest Pb^{2+} concentration. After 10 min, there was a rather continuous thickness decrease with increasing $[Pb^{2+}]$; after 60 min similar thicknesses were obtained at $[Pb^{2+}] \leq 30$ mM and a marked drop was seen only for $[Pb^{2+}] = 100$ mM. In a previous study, performed with compact PbO_2 layers and Pb^{2+}-free Mn^{2+} solutions [18], we observed that the secondary layer thickness, after growing as the square root of reaction time, attained a plateau value after ca. 60 min. The present data are compatible with a similar behavior at low Pb^{2+} concentration.

$PbO_2/Mn_xPb_{(1-x)}O_2$ samples were further characterized using EDS and XPS. Fig. 4a shows the compositions measured by EDS, after displacement reactions lasting 10 or 60 min, respectively, as a function

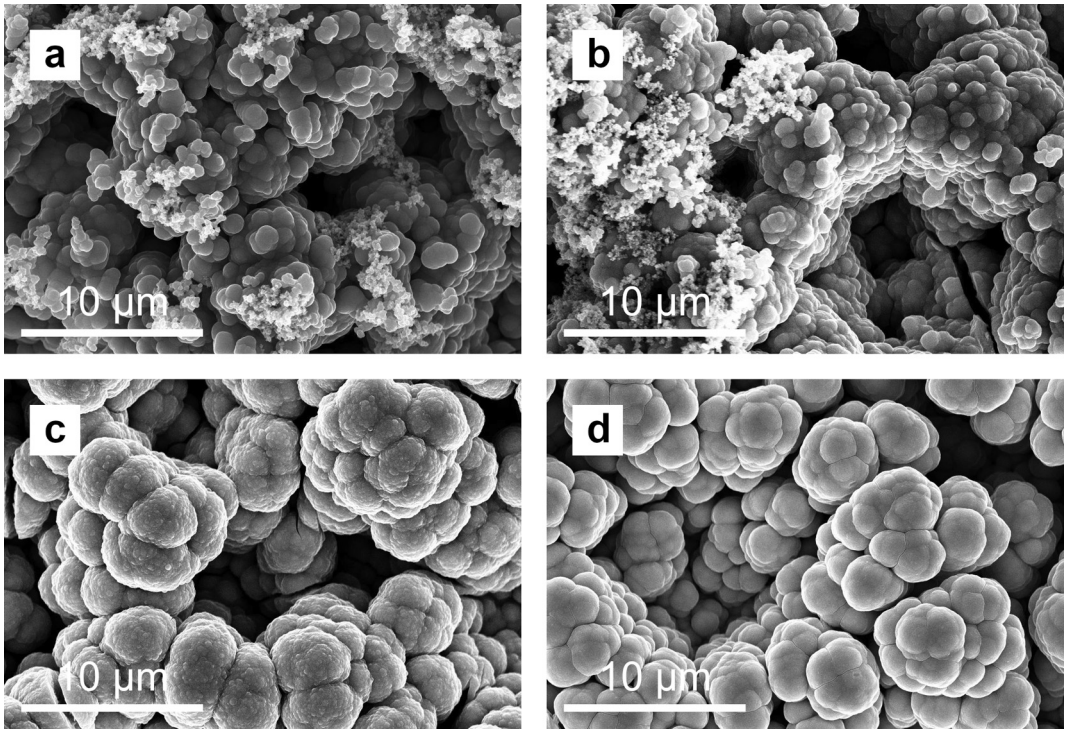

Fig. 1. SEM images of $PbO_2/Mn_xPb_{(1-x)}O_2$ samples prepared by reacting porous PbO_2 with acetate buffer solutions containing 0.2 M Mn^{2+} ions, in the absence (a) or in the presence of Pb^{2+} ions at 10 mM (b), 30 mM (c) or 100 mM (d) concentrations. Duration of the galvanic displacement reaction 60 min.

of [Pb^{2+}]. We have already reported that, as long as the sampling depth of the analysis was larger than the thickness of the secondary layer, the measured metal percentages accounted for both sacrificial and secondary layers, with the PbO_2 contribution progressively decreasing as the $Mn_xPb_{(1-x)}O_2$ layer thickness increased. This is the reason why, at all [Pb^{2+}] values, larger Mn percentages were measured after longer displacement reactions. However, the most important effect highlighted by Fig. 4a is that, for both reaction durations, the Mn percentage steadily decreased with increasing [Pb^{2+}]. Taking into account the lower thickness of the secondary layers grown at higher [Pb^{2+}] (Fig. 3), which induced overestimation of the Pb content, the results in Fig. 4a were not sufficient to conclude that secondary mixed oxides richer in Pb were formed at higher [Pb^{2+}].

Fig. 4b shows that when the surface compositions of $PbO_2/Mn_xPb_{(1-x)}O_2$ samples were measured by XPS, only very minor differences, compatible with experimental error and sample-to-sample variability, were detected for different reaction durations (10 or 60 min). This result strongly suggests that, at least between 10 and 60 min, the composition of the secondary $Mn_xPb_{(1-x)}O_2$ layers did not change significantly during their growth, so they had uniform composition along their thickness. A decreasing trend of Mn percentage with increasing [Pb^{2+}] was still observed with XPS, but it was less marked than suggested by EDS analyses. Clearly, due to the low sampling depth, much below the secondary oxide thickness (Fig. 3), the compositions measured with XPS were free from distortions caused by different thicknesses, while those measured with EDS were not. Thus, the progressive increase in composition differences between 60-min- and 10-min-samples for increasing [Pb^{2+}], shown in Fig. 4a, could be ascribed to a slower growth of the secondary oxide thickness at higher [Pb^{2+}] (Fig. 3).

Fig. 4c compares the secondary oxides compositions measured with either EDS or XPS on samples prepared with 60-min displacement reactions and shows that both techniques provided essentially identical results. It may be concluded that, once the secondary layer thickness reached or exceeded the sampling depth of EDS, the true composition of the secondary mixed Mn-Pb oxides could be reliably measured by both EDS and XPS techniques, in spite of their very different sampling depth.

The whole set of results presented in Figs. 1 to 4 leads to the following conclusions:

(i) In the presence of progressively higher concentrations of Pb^{2+} ions in the Mn^{2+} solutions, secondary mixed oxides $Mn_xPb_{(1-x)}O_2$ with progressively lower values of x were formed.
(ii) Higher concentrations of Pb^{2+} (≥30 mM) depressed the secondary oxide growth rate. This result is in agreement with our previous conclusion that the diffusion of Pb species from the sacrificial oxide to the solution, across the $Mn_xPb_{(1-x)}O_2$ layer, controlled the overall rate [18]. It also suggests that the transfer of Pb species across the interface between $Mn_xPb_{(1-x)}O_2$ and the solution was reversible.
(iii) The presence of Pb^{2+} ions at low concentrations (≤10 mM) had negligible effects on the secondary oxide morphology, thickness and composition, confirming *a posteriori* that one could disregard memory effects associated with accumulation of Pb^{2+} ions which, in any case, never exceeded a 1 mM concentration.

Due to the amorphous nature of secondary oxides, we were unable to collect evidence of the possible formation of compounds with well-defined stoichiometry.

3.2. PbO_2-Mn^{2+} reaction – Chronopotentiometry

Fig. 5a shows chronopotentiometric curves recorded during galvanic displacement reactions, carried out with Mn^{2+} solutions containing Pb^{2+} ions at variable concentrations. All curves had common features: (i) an initial part, where the open circuit potential (E_{OC}) decreased significantly, from ca. 1.25 V to ≤ 0.95 V vs. SHE, (ii) an intermediate part, where E_{OC} fluctuated and (iii) a final part, where E_{OC} was quasi-independent of the reaction duration, in agreement with

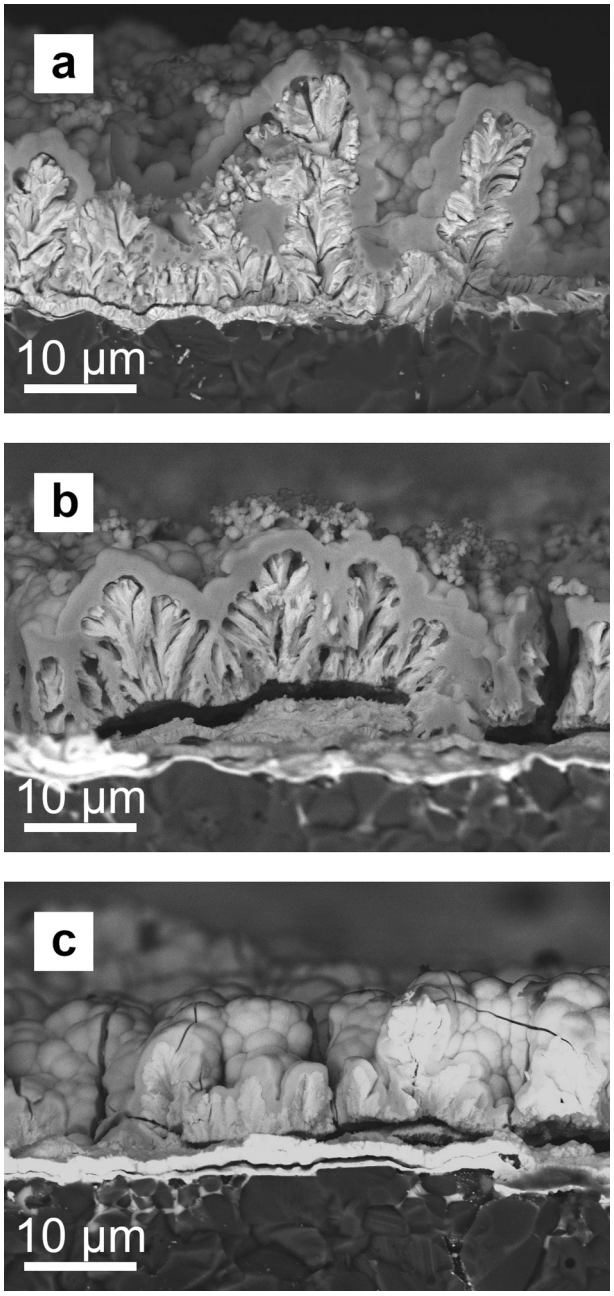

Fig. 2. Cross-sectional SEM images of $PbO_2/Mn_xPb_{(1-x)}O_2$ samples prepared by reacting porous PbO_2 with acetate buffer solutions containing 0.2 M Mn^{2+} ions and Pb^{2+} ions at 1 mM (a), 10 mM (b) and 100 mM (c) concentrations. Duration of the galvanic exchange reaction 60 min.

previous results [16,18]. All these features were influenced by the concentration of Pb^{2+}. E_{OC} decreased progressively less sharply and stabilized at higher values, as $[Pb^{2+}]$ increased, while the fluctuations occurred on a longer time scale.

Fig. 5b shows that the E_{OC} values recorded after 60 min, henceforth denoted E_{60min}, in the presence of 0.2 M Mn^{2+}, increased monotonously with $[Pb^{2+}]$, by ca. 75 mV per $[Pb^{2+}]$ decade. Fig. S3a (Supplementary information) compares E_{60min} values measured in two independent series of experiments, showing that those values were quite well-defined. For the sake of comparison, chronopotentiometric curves were recorded during the immersion of PbO_2 samples in Mn^{2+}-free acetate buffers containing 1, 10 or 100 mM Pb^{2+} (pH 4.8, 25 °C). In this case, E_{OC} decreased only slightly with time and

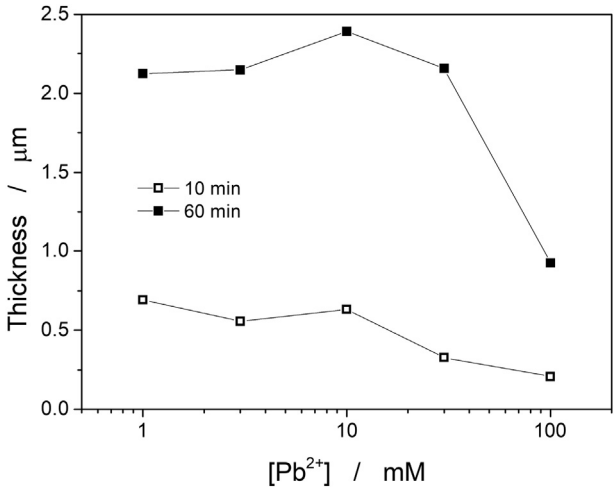

Fig. 3. Dependence of the thickness of $Mn_xPb_{(1-x)}O_2$ secondary layers on the concentration of Pb^{2+} ions in the Mn^{2+} acetate buffer solution. Secondary layers were grown onto porous PbO_2 during 10 or 60 min, as indicated on the figure.

Fig. 5b shows that E_{60min} stabilized at values that became lower when $[Pb^{2+}]$ increased, with a slope not far from the theoretical value (29.5 mV per $[Pb^{2+}]$ decade). The measured E_{OC} values were ca. 100 mV higher than those computed according to the Nernst equation for acetate-free water solutions [23]. Thus, increasing $[Pb^{2+}]$ induced E_{60min} variations in opposite directions in Mn^{2+}-containing solutions, where PbO_2 underwent galvanic displacement, and in Mn^{2+}-free solutions, where PbO_2 did not undergo redox reactions.

To rationalize the E_{60min} dependence on $[Pb^{2+}]$, one may hypothesize that the almost stable values measured after long reaction time were equilibrium potentials. In analogy with the equilibria of individual oxides, PbO_2 and MnO_2, with their respective bivalent cations, one may write for a mixed oxide $Mn_xPb_{(1-x)}O_2$:

$$Mn_xPb_{(1-x)}O_2 + 2e^- + 4H^+ = xMn^{2+} + (1-x)Pb^{2+} + 2H_2O \quad (2)$$

The corresponding Nernst equation, using concentrations instead of activities, is:

$$E_{eq} = E^0_{mix} + \frac{RT}{2F} ln \frac{[H^+]^4}{[Mn^{2+}]^x [Pb^{2+}]^{(1-x)}} \quad (3)$$

where E^0_{mix} is the standard potential of the mixed oxide, which depends on x. Eq. (3) agrees with the approach proposed by Heusler for multicomponent electrodes [24], also discussed by Zangari [25] with reference to metal alloys electrodeposition. To the best of our knowledge, E^0_{mix} values for Mn-Pb oxides with variable x are not known. As a first approximation, one may consider a linear combination

$$E^0_{mix} = xE^0_{Mn} + (1-x)E^0_{Pb} \quad (4)$$

$$E_{eq} = xE^0_{Mn} + (1-x)E^0_{Pb} + \frac{RT}{2F} ln \frac{[H^+]^4}{[Mn^{2+}]^x [Pb^{2+}]^{(1-x)}} \quad (5)$$

According to Eq. (5), the x value affects E_{eq} in two ways, i.e. via E^0_{mix} (which decreases for increasing x because $E^0_{Mn} < E^0_{Pb}$) and via the logarithmic term (in which both $[Pb^{2+}]$ and x vary). Equation (5) reduces to the correct Nernst equations for individual oxides when $x = 0$ or $x = 1$. However, a linear variation of E^0_{mix} with x corresponds to assuming no interactions between individual oxides in the formation of $Mn_xPb_{(1-x)}O_2$, i.e. to assuming the free energy of mixing to be zero, so Eq. (4) and (5) are not expected to be fully accurate. Nevertheless,

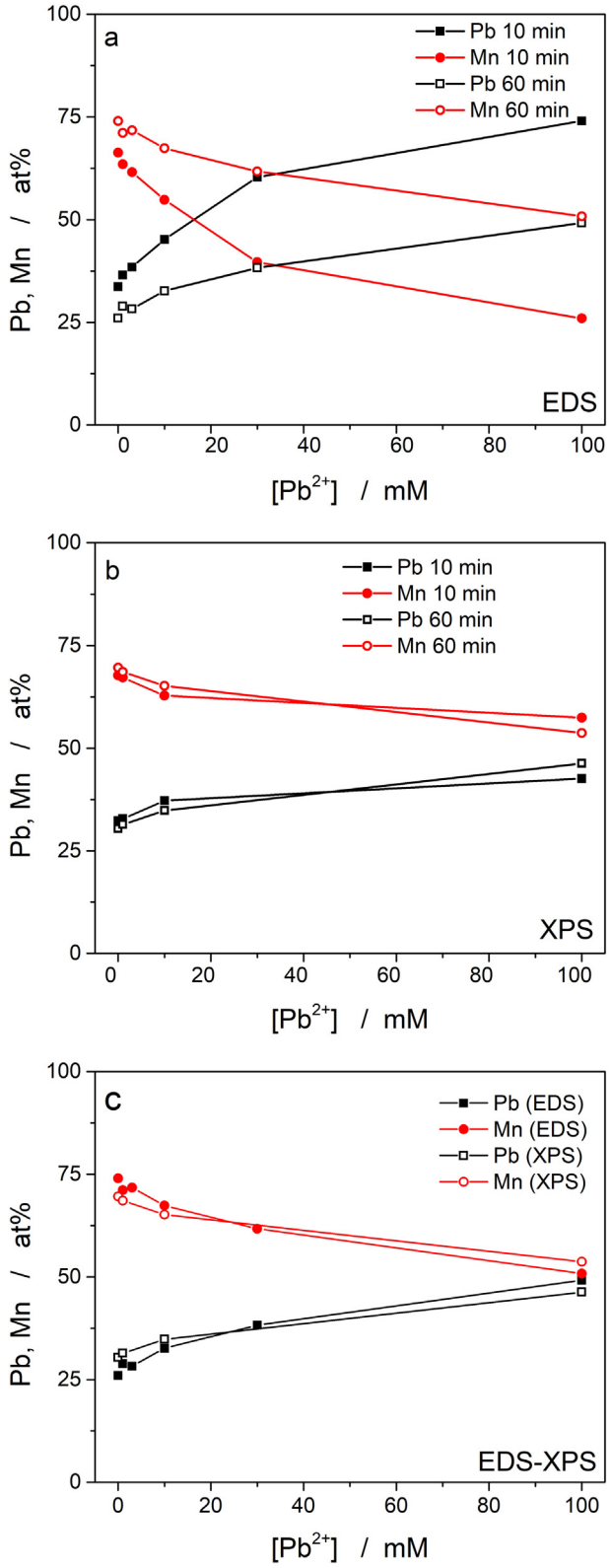

Fig. 4. Composition of the secondary oxides obtained by reaction of porous PbO_2 with 0.20 M $Mn(CH_3COO)_2$, 0.20 M CH_3COOH solutions (pH 4.8, 25 °C), as a function of the concentration of Pb^{2+} ions. Effect of the duration of the galvanic displacement reaction on the composition measured by EDS (a) or XPS (b). Comparison between compositions measured by EDS and XPS on samples obtained with 60 min galvanic exchange reactions (c). Percentages of Mn and Pb refer to metal atoms only.

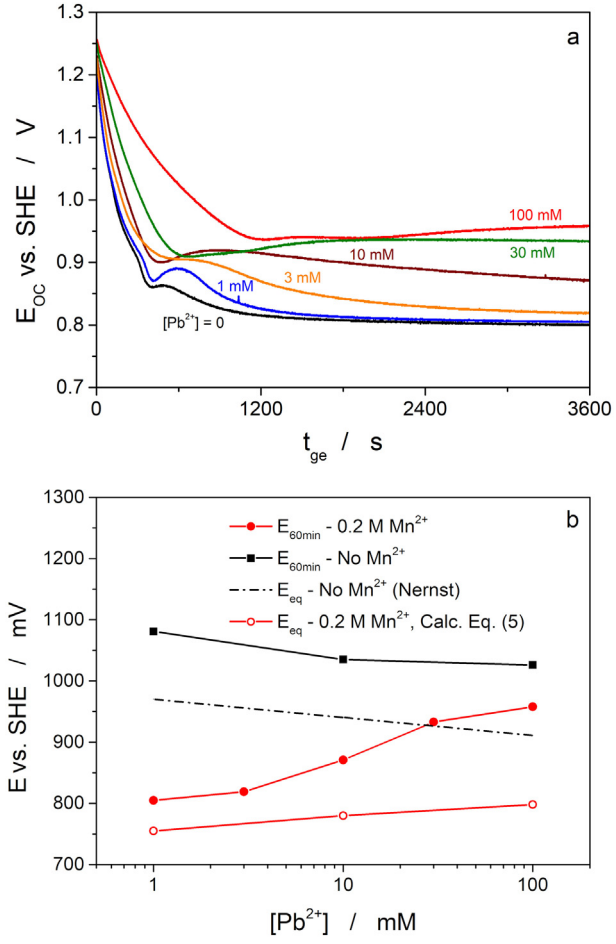

Fig. 5. (a) Chronopotentiograms recorded during galvanic displacement reactions between PbO_2 layers and 0.20 M $Mn(CH_3COO)_2$, 0.20 M CH_3COOH solutions (pH 4.8, 25 °C), containing Pb^{2+} ions at the indicated concentrations. (b) Dependence on the Pb^{2+} concentration of the open circuit potential measured after 60 min either in 0.2 M Mn^{2+} acetate solutions or in Mn^{2+}-free acetate solutions. The dash-dot line is calculated according to the Nernst equation, neglecting possible effects of acetate ions. The E values shown as empty circles are calculated according to Eq. (5).

Eq. (5) may be used for a first-approximation calculation of E_{eq} values to be compared with experimental E_{60min} values. Table 1 summarizes the results of such a calculation, made using the following values: $E^0_{Mn} = 1.228V$ and $E^0_{Pb} = 1.449V$, both vs. SHE [23], $[H^+] = 10^{-4.8}$ M and the x values determined in the EDS and XPS analyses which, as shown in Fig. 4c, provided almost identical quasi-bulk and surface compositions of secondary mixed oxides.

The E_{eq} values calculated according to Eq. (5) are shown in Fig. 5b as empty circles. These values are always lower than the experimental E_{60min} values, but they increase for increasing concentration of Pb^{2+} in solution, like the experimental ones, though with a weaker slope. The

Table 1
Equilibrium potentials for the reduction of Mn-Pb mixed oxides, calculated according to Eq. (5), with $[Mn^{2+}] = 0.2$ M and pH = 4.8, and comparison with experimental E_{60min} values.

$[Pb^{2+}]$/M	x	E_{eq}/V vs. SHE	E_{60min}/V vs. SHE
10^{-3}	0.75	0.755	0.807
10^{-2}	0.63	0.780	0.877
10^{-1}	0.50	0.798	0.947

calculation according to Eq. (5) leads to this result because the composition of the mixed oxide, i.e. the x value, influences E_{eq} mainly via E^0_{mix}. Both in the presence and in the absence of Mn^{2+} in solution, calculations based on Nernst equation yield values lower than those experimentally observed, with a difference of the order of 100 mV. It is probable that, in both cases, neglecting the effect of acetate ions caused these comparable shifts. In Fig. S3b, the curve calculated according to Eq. (5) has been shifted upward by 100 mV, to pictorially show the level of (dis)agreement between experiments and calculations.

Fig. 5a shows that the initial sharp decrease of E_{OC} occurred during a few minutes in solutions without Pb^{2+} and progressively extended to reach ca. 20 min in 100 mM Pb^{2+} solutions. However, Fig. 3 shows that the secondary oxide thickness kept increasing beyond these initial periods, at all [Pb^{2+}]. One may conclude that the initial E_{OC} decrease was due to the formation of mixed oxide which composition changed in time, to approach and finally reach the equilibrium one, but the secondary oxide growth continued, through the progressive consumption of PbO_2 and its replacement by $Mn_xPb_{(1-x)}O_2$ with an essentially constant x, during the intermediate period where fluctuations were observed.

3.3. PbO_2-Co^{2+} reaction

The reaction between PbO_2 and Co^{2+}, to form mixed oxides may be written:

$$PbO_2 + 3yCo^{2+} + 2yH_2O \rightarrow [Co_3O_4]_y[PbO_2]_{(1-y)} + yPb^{2+} + 4yH^+ \quad (6)$$

For further details see Supplementary Information. Fig. 6a shows the oxides' composition measured using EDS (full symbols) or XPS (empty symbols), after 60-minute galvanic displacement reactions, as a function of [Pb^{2+}]. As observed for the PbO_2-Mn^{2+} system, data show that the secondary oxides became richer in Pb when [Pb^{2+}] increased. For the same [Pb^{2+}], the Pb content was lower in Co-Pb than in Mn-Pb mixed oxides, in agreement with observation reported in [18] for Pb^{2+}-free solutions.

Fig. 6b shows that the thickness of the secondary oxide increased from ca. 750 nm to almost 1.5 μm, i.e. the average growth rate increased from 12.5 to 25 nm min^{-1}, when [Pb^{2+}] varied from 1 to 100 mM. Cross-sectional SEM images of two samples are shown in the Supplementary Information (Fig. S4), together with images of the samples' outer surface, which reveal conformal growth of the secondary mixed oxide. The Co percentages measured with XPS were higher than those obtained with EDS because, due to the relatively low thickness of secondary oxides, EDS sampled significant amounts of unreacted PbO_2. The increased thickness of the secondary oxide at high [Pb^{2+}] was not sufficient to lead the EDS and XPS data to converge.

Comparison of Figs. 3 and 6b reveals opposite thickness-[Pb^{2+}] trends for the PbO_2-Mn^{2+} and PbO_2-Co^{2+} systems. This result was unexpected because, if the rate of the galvanic displacement reaction was controlled by the diffusion of Pb species across the secondary mixed oxide, as we proposed in reference [18] with the support of experimental evidence, an increase in the concentration of Pb^{2+} in the reaction medium should have slowed down the process. However, this line of reasoning assumes that the properties of the secondary mixed oxide were independent of its composition, i.e. independent of Pb content. Such an assumption may be correct or not for different mixed oxides and in different ranges of composition. In our tentative explanation of the observed thickness-[Pb^{2+}] trends, we propose that it was correct for $Mn_xPb_{(1-x)}O_2$ and incorrect for $(Co_3O_4)_y(PbO_2)_{(1-y)}$. Thus, in agreement with our previous findings [18], we maintain that for both systems the secondary oxides grew under diffusion control. However, different behavior might result from different effects of the mixed oxide composition on the diffusivity of the Pb species (D_{Pb}). It is plausible that in the Pb-Mn oxides, changes in composition

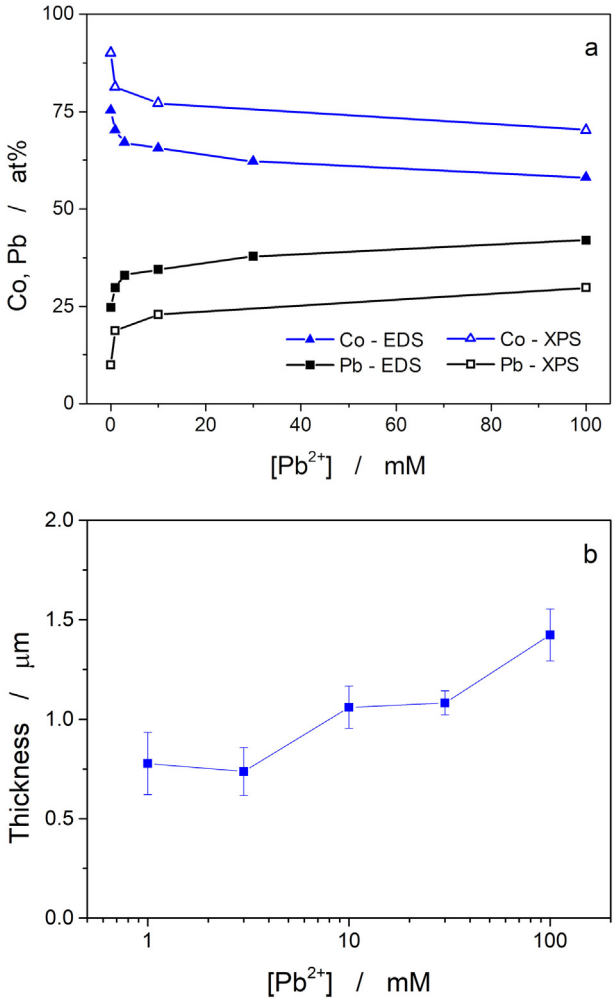

Fig. 6. Dependence of the secondary oxide composition (a) and thickness (b) measured after 60-minute between PbO_2 and Co^{2+}. Compositions were measured using both EDS (full symbols) and XPS (empty symbols).

influenced D_{Pb} very little, thus higher [Pb^{2+}] values, corresponding to lower gradients, depressed the growth rate. Instead, in the Pb-Co oxides, where metal/oxygen ratios were different for Pb and Co, changes in composition were likely to induce higher levels of disorder in the mixed oxides richer in Pb (the minority metal). As a consequence, Pb-richer mixed oxides became more permeable to Pb species, D_{Pb} was enhanced and, despite lower gradients, faster growth occurred.

Fig. 7a shows that chronopotentiometric curves recorded during the PbO_2-Co^{2+} reaction were not very strongly affected by [Pb^{2+}]. The essentially stable E_{OC} values measured at long reaction time varied in a narrow range. Fig. 7b (full points) shows that E_{60min} values decreased for increasing [Pb^{2+}], i.e. they varied in the opposite direction with respect to the PbO_2-Mn^{2+} system.

In analogy with the previous section, we calculated the equilibrium potentials for the reduction of the Co-Pb mixed oxide to Co^{2+} and Pb^{2+}, and compared them with the E_{60min} values. Due to the different metal/oxygen ratios in Co_3O_4 and PbO_2, the Co-Pb mixed oxide is conveniently written $(Co_3O_4)_y(PbO_2)_{(1-y)}$. Its reduction reaction is:

$$(Co_3O_4)_y(PbO_2)_{(1-y)} + 2e^- + (4y+4)H^+ = 3yCo^{2+} + (1-y)Pb^{2+} + (2y+2)H_2O \quad (7)$$

In this equation, y does not coincide with $X_{Co} = \frac{Co}{Co+Pb}$, the molar fraction of Co in the mixed oxide (referred to metal atoms only). The link between y and X_{Co} is given by

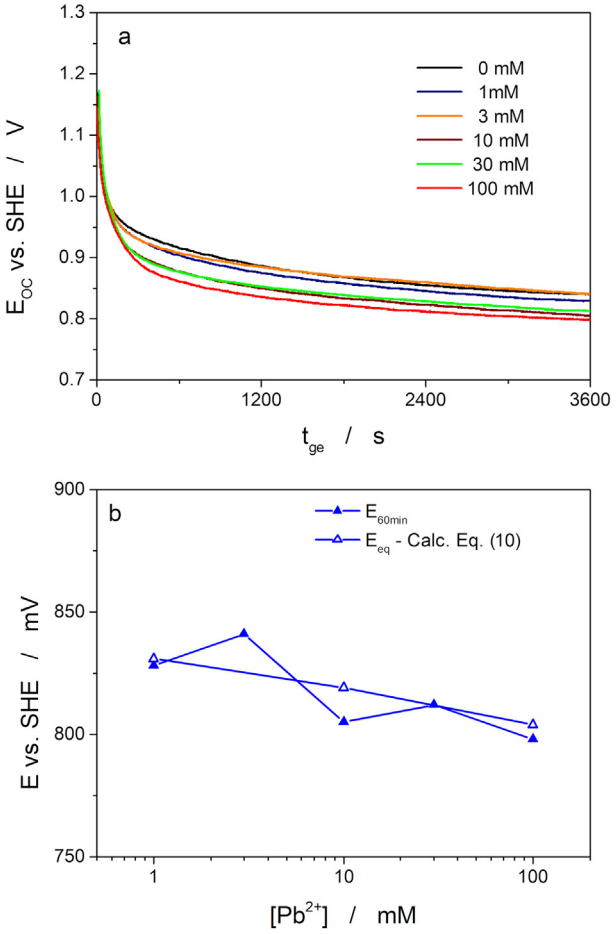

Fig. 7. (a) Chronopotentiograms recorded during galvanic displacement reactions between PbO_2 and Co^{2+} in acetate solutions containing Pb^{2+} ions at the indicated concentrations. (b) Effect of the Pb^{2+} concentration on the open circuit potential measured after 60 min, full points, and on the equilibrium potential of reaction (6) calculated according to Eq. (10), empty points.

$$y = \frac{X_{Co}}{3 - 2X_{Co}} \tag{8}$$

The Nernst equation for reaction (7), using concentrations instead of activities, is:

$$E_{eq} = E^0_{mix} + \frac{RT}{2F} ln \frac{[H^+]^{(4y+4)}}{[Co^{2+}]^{3y}[Pb^{2+}]^{(1-y)}} \tag{9}$$

which converts to Eq. (10)

$$E_{eq} = yE^0_{Co} + (1-y)E^0_{Pb} + \frac{RT}{2F} ln \frac{[H^+]^{(4y+4)}}{[Co^{2+}]^{3y}[Pb^{2+}]^{(1-y)}} \tag{10}$$

if one assumes, as in the previous section, that E^0_{mix} is given by the linear combination of the E^0 values relevant to individual oxides.

We calculated E_{eq} values for the PbO_2-Co^{2+} system, using Eq. (10), E^0_{Co} = 2.112 V vs. SHE [26], the temperature coefficients reported by Bratsch [27], to take into account that the reaction temperature was 75 °C, and the y values obtained from XPS analyses. Since Bratsch's paper did not include Co_3O_4, the temperature coefficient of Co_2O_3 was used. Calculated E_{eq} and experimental E_{60min} values are compared in Fig. 7b and in Table 2. The calculation reproduces the experimentally observed decrease of E_{60min} with increasing $[Pb^{2+}]$, yielding values that are close to the experimental ones.

Table 2
Equilibrium potentials for the reduction of Co-Pb mixed oxides, calculated according to Eq. (10), with $[Co^{2+}]$ = 0.2 M and pH = 4.8, and comparison with experimental E_{60min} values.

$[Pb^{2+}]$/M	X_{Co} [a]	y	E_{eq}/V vs. SHE	E_{60min}/V vs. SHE
10^{-3}	0.81	0.59	0.831	0.828
10^{-2}	0.77	0.53	0.819	0.805
10^{-1}	0.70	0.44	0.804	0.798

[a] $X_{Co} = \frac{Co}{Co+Pb}$ is the molar fraction of Co in the mixed oxide (referred to metal atoms only) as determined using XPS (See Fig. 6a).

4. Conclusions

We have studied the effect of concentration of Pb^{2+} ions present in solution on morphology, thickness and composition of the secondary mixed oxide layers formed in galvanic displacement reactions between PbO_2 and either Mn^{2+} or Co^{2+} cations. Both analogies and differences were observed for the two systems.

- When the concentrations of Pb^{2+} in the reaction media was increased, secondary oxides richer in Pb were obtained in both PbO_2-Mn^{2+} and PbO_2-Co^{2+} reactions. Even using Pb^{2+}-free solutions, the secondary layers consisted of mixed oxides with Pb contents that could not be decreased at will.
- During the galvanic exchange reactions, the open circuit potential decreased for both PbO_2-Mn^{2+} and PbO_2-Co^{2+} systems. However, when $[Pb^{2+}]$ increased, the steady value obtained at long time increased for PbO_2-Mn^{2+}, but decreased for PbO_2-Co^{2+}. These divergent trends were both reproduced through approximate calculations of equilibrium potentials, based on identical approaches (see Eq. (2)-(5) for Mn^{2+} and Eq. (7)-(10) for Co^{2+}).
- When $[Pb^{2+}]$ increased, the secondary oxide thickness attained at a fixed reaction time decreased for PbO_2-Mn^{2+}, but increased for PbO_2-Co^{2+}. A tentative explanation of these opposite trends assumes that the diffusivity of the Pb species, the transport of which controlled the growth rate, was essentially independent of the composition of the Mn-Pb mixed oxide, but increased significantly with the Pb content in the Co-Pb mixed oxide, due to more profound disordering.

Besides allowing us to elucidate new aspects of the little-known mechanisms of oxide-oxide galvanic displacement reactions [28], the present study has also shown that the accumulation of Pb^{2+} ions released by the reduction of PbO_2 in initially Pb^{2+}-free reaction media could be neglected because Pb^{2+} concentrations of the order of 1 mM or lower had no detectable effect on morphology, composition and thickness of the secondary oxides, under the typical conditions used in our experiments.

The significantly different behavior observed with PbO_2-Mn^{2+} and PbO_2-Co^{2+} systems suggests that investigating other cations might be interesting. Such investigation is beyond the scope of the present paper, but additional work is planned.

CRediT authorship contribution statement

Nicola Comisso: Investigation. **Lidia Armelao:** Writing - review & editing. **Sandro Cattarin:** Writing - review & editing. **Stefano Fasolin:** Investigation. **Luca Mattarozzi:** Investigation. **Marco Musiani:** Conceptualization, Supervision, Writing - original draft, Writing - review & editing. **Marzio Rancan:** Investigation. **Lourdes Vázquez-Gómez:** Investigation. **Enrico Verlato:** Investigation.

Declaration of Competing Interest

The authors declare that they have no known competing financial interests or personal relationships that could have appeared to influence the work reported in this paper.

Acknowledgments

Financial support from the Italian Government, Ministry of Education, Universities and Research – MIUR (PRIN N° 2017MCEEY4 funding) is gratefully acknowledged.

Appendix A. Supplementary data

Supplementary data to this article can be found online at https://doi.org/10.1016/j.jelechem.2021.115199.

References

[1] M. Paunovic, M. Schlesinger, Fundamentals of Electrochemical Deposition, John Wiley & Sons Inc., New York, 1998, pp. 161–166. chapter 9.
[2] X. Xia, Y. Wang, A. Ruditskiy, Y. Xia, 25th Anniversary article: galvanic replacement: a simple and versatile route to hollow nanostructures with tunable and well-controlled properties, Adv. Mater. 25 (2013) 6313.
[3] X. Wang, J. Feng, Y. Bai, Q. Zhang, Y. Yin, Synthesis, properties, and applications of hollow micro-/nanostructures, Chem. Rev. 116 (2016) 10983.
[4] Z. Wang, D. Luan, C.M. Li, F. Su, S. Madhavi, F.Y.C. Boey, X.W. Lou, Engineering nonspherical hollow structures with complex interiors by template-engaged redox etching, J. Am. Chem. Soc. 132 (2010) 16272–16277.
[5] M.H. Oh, T. Yu, S.-H. Yu, B. Lim, K.-T. Ko, M.G. Willinger, D.-H. Seo, B.H. Kim, M. G. Cho, J.-H. Park, K. Kang, Y.-E. Sung, N. Pinna, T. Hyeon, Galvanic replacement reactions in metal oxide nanocrystals, Science 340 (2013) 964–968.
[6] H.-M. Jeong, J.-H. Kim, S.-Y. Jeong, C.-H. Kwak, J.-H. Lee, $Co_3O_4-SnO_2$ hollow heteronanostructures: facile control of gas selectivity by compositional tuning of sensing materials via galvanic replacement, ACS Appl. Mater. Interfaces 8 (2016) 7877–7883.
[7] A. López-Ortega, A.G. Roca, P. Torruella, M. Petrecca, S. Estrade´, F. Peiro´, V. Puntes, J. Nogués, Galvanic replacement onto complex metal-oxide nanoparticles: impact of water or other oxidizers in the formation of either fully dense onion-like or multicomponent hollow MnO_x/FeO_x structures, Chem. Mater. 28 (2016) 8025–8031.
[8] M. Diab, T. Mokari, Role of the counteranions on the formation of different crystal structures of iron oxyhydroxides via redox reaction, Cryst. Growth Des. 17 (2017) 527–533.
[9] H.B. Wu, J.S. Chen, H.H. Hng, X.W. Lou, Nanostructured metal oxide-based materials as advanced anodes for lithium-ion batteries, Nanoscale 4 (2012) 2526–2542.
[10] D.-G. Lee, S.M. Kim, S.M. Kim, S.W. Lee, J.Y. Park, K. An, I.S. Lee, Postsynthesis modulation of the catalytic interface inside a hollow nanoreactor: exploitation of the bidirectional behavior of mixed-valent Mn_3O_4 phase in the galvanic replacement reaction, Chem. Mater. 28 (2016) 9049–9055.
[11] J.-S. Jang, W.-T. Koo, S.-J. Choi, I.-D. Kim, Metal organic framework-templated chemiresistor: sensing type transition from P-to-N using hollow metal oxide polyhedron via galvanic replacement, J. Am. Chem. Soc. 139 (2017) 11868–11876.
[12] J. Lim, J.M. Lee, B. Park, X. Jin, S.-J. Hwang, Homogeneous cationic substitution for two-dimensional layered metal oxide nanosheets via a galvanic exchange reaction, Nanoscale 9 (2017) 792–801.
[13] L. Zhang, G. Wang, F. Yu, Y. Zhang, B.-C. Ye, Y. Li, Facile synthesis of hollow $MnFe_2O_4$ nanoboxes based on galvanic replacement reaction for fast and sensitive VOCs sensor, Sensors Actuators B 258 (2018) 589–596.
[14] H.-W. Yeh, C.-J. Chang, G.G. Huang, P.-Y. Chen, Electrochemical conversion of ionic liquid-lead sulfate paste into metallic lead or lead(IV) oxide: Extracting lead from water-insoluble lead salt and formation of cobalt oxide electrocatalyst via galvanic displacement, J. Electroanal. Chem. 834 (2019) 64–70.
[15] J.-S. Jang, S.-E. Lee, S.-J. Choi, W.-T. Koo, D.-H. Kim, H. Shin, H.J. Park, I.-D. Kim, Heterogeneous, porous 2D oxide sheets via rapid galvanic replacement: toward superior HCHO sensing application, Adv. Funct. Mat. 29 (2019) 1903012.
[16] N. Comisso, L. Armelao, S. Cattarin, P. Guerriero, L. Mattarozzi, M. Musiani, M. Rancan, L. Vázquez-Gómez, E. Verlato, Preparation of porous oxide layers by oxygen bubble templated anodic deposition followed by galvanic displacement, Electrochim. Acta 253 (2017) 11–20.
[17] N. Comisso, L. Armelao, S. Cattarin, P. Guerriero, L. Mattarozzi, M. Musiani, M. Rancan, L. Vázquez-Gómez, E. Verlato, Porous oxide electrocatalysts for oxygen evolution reaction prepared through a combination of hydrogen bubble templated deposition, oxidation and galvanic displacement steps, Electrochim. Acta 273 (2018) 454–461.
[18] N. Comisso, M. Rancan, L. Armelao, S. Barison, S. Cattarin, P. Guerriero, L. Mattarozzi, M. Musiani, L. Vázquez-Gómez, E. Verlato, Investigation on the oxide-oxide galvanic displacement reactions employed in the preparation of electrocatalytic layers, Electrochim. Acta 341 (2020) 136056.
[19] N. Comisso, L. Armelao, S. Cattarin, S. Fasolin, L. Mattarozzi, M. Musiani, M. Rancan, L. Vázquez-Gómez, E. Verlato, Deposition of FeOOH layers onto porous PbO_2 by galvanic displacement and their use as electrocatalysts for oxygen evolution reaction, J. Electroanal. Chem. 114844 (2021).
[20] N. Comisso, S. Cattarin, P. Guerriero, L. Mattarozzi, M. Musiani, E. Verlato, Oxygen bubble–templated anodic deposition of porous PbO_2, Electrochem. Commun. 60 (2015) 144–147.
[21] N. Comisso, S. Cattarin, P. Guerriero, L. Mattarozzi, M. Musiani, E. Verlato, Electrochemical behaviour of porous PbO_2 layers prepared by oxygen bubble templated anodic deposition, Electrochim. Acta 200 (2016) 259–267.
[22] N. Comisso, S. Cattarin, P. Guerriero, L. Mattarozzi, M. Musiani, E. Verlato, Conversion of porous PbO_2 layers through galvanic displacement reaction with Mn^{2+} ions, Electrochem. Commun. 73 (2016) 59–62.
[23] M. Pourbaix, Atlas D'Equilibres Electrochimiques, Gauthier-Villars & Cie, Paris, 1963, pp. 485–493.
[24] K.E. Heusler, Multicomponent electrodes, Electrochim. Acta 41 (1995) 411–418.
[25] G. Zangari, Electrodeposition of alloys and compounds in the era of microelectronics and energy conversion technology, Coatings 5 (2015) 195–218.
[26] M. Pourbaix, Atlas D'Equilibres Electrochimiques, Gauthier-Villars & Cie, Paris, 1963, pp. 322–329.
[27] S.G. Bratsch, Standard electrode potentials and temperature coefficients in water at 298.15 K, J. Phys. Chem. Ref. Data 18 (1989) 1–21.
[28] M.J. Lawrence, A. Kolodziej, P. Rodriguez, Controllable synthesis of nanostructured metal oxide and oxyhydroxide materials via electrochemical methods, Curr. Opin. Electrochem. 10 (2018) 7–15.